AGU100 ADVANCING EARTH AND SPACE SCIENCE

JGR Space Physics

RESEARCH ARTICLE
10.1029/2018JA026344

Plasma Transport in Saturn's Low-Latitude Ionosphere: Cassini Data

T. E. Cravens[1], M. Morooka[2], A. Renzaglia[1], L. Moore[3], J. H. Waite Jr.[4], R. Perryman[4], M. Perry[5], J.-E. Wahlund[2], A. Persoon[6], and L. Hadid[2]

[1]Department of Physics and Astronomy, University of Kansas, Lawrence, KS, USA, [2]Swedish Institute of Space Physics, Uppsala, Sweden, [3]Center for Space Physics, Boston University, Boston, MA, USA, [4]Space Science and Engineering Division, Southwest Research Institute, San Antonio, TX, USA, [5]Applied Physics Laboratory, The Johns Hopkins University, Laurel, MD, USA, [6]Department of Physics and Astronomy, University of Iowa, Iowa City, IA, USA

Key Points:
- First in situ ion flow measurements in an outer planet ionosphere are shown
- Protons dominate Saturn's equatorial topside ionosphere, and Cassini data showed that they flow from the Northern to the southern hemisphere
- The Cassini Ion and Neutral Mass Spectrometer measured proton flow speeds in Saturn's ionosphere as high as 3 km/s

Supporting Information:
- Supporting Information S1
- Data Set S1
- Data Set S2
- Data Set S3
- Data Set S4
- Data Set S5
- Data Set S6
- Data Set S7
- Data Set S8

Correspondence to:
T. E. Cravens,
cravens@ku.edu

Citation:
Cravens, T. E., Morooka, M., Renzaglia, A., Moore, L., Waite, J. H., Jr., Perryman, R., et al. (2019). Plasma transport in Saturn's low-latitude ionosphere: Cassini data. *Journal of Geophysical Research: Space Physics*, *124*, 4881–4888. https://doi.org/10.1029/2018JA026344

Received 3 DEC 2018
Accepted 7 MAY 2019
Accepted article online 20 MAY 2019
Published online 29 JUN 2019

Abstract In 2017 the Cassini Orbiter made the first in situ measurements of the upper atmosphere and ionosphere of Saturn. The Ion and Neutral Mass Spectrometer in its ion mode measured densities of light ion species (H^+, H_2^+, H_3^+, and He^+), and the Radio and Plasma Wave Science instrument measured electron densities. During proximal orbit 287 (denoted P287), Cassini reached down to an altitude of about 3,000 km above the 1 bar atmospheric pressure level. The topside ionosphere plasma densities measured for P287 were consistent with ionospheric measurements during other proximal orbits. Spacecraft potentials were measured by the Radio and Plasma Wave Science Langmuir probe and are typically about negative 0.3 V. Also, for this one orbit, Ion and Neutral Mass Spectrometer was operated in an instrument mode allowing the energies of incident H^+ ions to be measured. H^+ is the major ion species in the topside ionosphere. Ion flow speeds relative to Saturn's atmosphere were determined. In the southern hemisphere, including near closest approach, the measured ion speeds were close to zero relative to Saturn's corotating atmosphere, but for northern latitudes, southward ion flow of about 3 km/s was observed. One possible interpretation is that the ring shadowing of the southern hemisphere sets up an interhemispheric plasma pressure gradient driving this flow.

1. Introduction

During 2017 the Cassini Orbiter made in situ measurements of the upper atmosphere and ionosphere of Saturn. Previously, only remote measurements of the atmosphere and ionosphere were made (cf. Kliore et al., 1980; Koskinen et al., 2015). The Cassini Ion and Neutral Mass Spectrometer (INMS) made measurements in its closed source neutral mode, demonstrating that molecular hydrogen and helium were the major neutral constituents (Waite et al., 2018). An exciting discovery was that a variety of other neutral gases (e.g., CH_4, H_2O, and hydrocarbons) and grains are transported from the inner rings to the upper atmosphere of Saturn (cf. Mitchell et al., 2018; Perry et al., 2018; Waite et al., 2018). The ionosphere is strongly affected by this influx of ring material (Cravens et al., 2018; Moore et al., 2018; Wahlund et al., 2018; Waite et al., 2018).

Only low mass (m/q less than 9) ion species were measured by the open source ion (OSI) mode of INMS during the proximal orbits due to the high spacecraft (s/c) speed (i.e., $v \approx$ of 31 km/s) with respect to the atmosphere. Several light ion species (H^+, H_2^+, H_3^+, and He^+) were detected, which was not surprising given models of the ionosphere (cf. Moore et al., 2018). Quantitatively the total light ion densities measured in the main ionosphere were much less than the measured electron density. The prevailing interpretation is that heavy molecular ion species are produced by the reaction of H^+ and H_3^+ ions with heavy neutral species entering the atmosphere from the rings (e.g., Cravens et al., 2018; Moore et al., 2018; Waite et al., 2018). However, in the topside ionosphere H^+ is the major ion species (Cravens et al., 2018; Waite et al., 2018).

It is well known for planetary ionospheres, including the Earth's, that the plasma density is controlled mainly by chemical processes at lower altitudes and by transport processes at higher altitudes where atmospheric densities are lower (Schunk & Nagy, 2009). The current paper focuses on the dynamics of the topside ionosphere of Saturn and describes measurements that indicate probable plasma flow from the northern hemisphere to the southern hemisphere, presumably along magnetic field lines. These measurements have a number of uncertainties but they are unique. A possible interpretation of the results is that the ring

shadowing of the southern hemisphere sets up an interhemispheric plasma pressure gradient driving this flow.

2. Instrument Descriptions

2.1. INMS Instrument and Techniques

The INMS instrument was a radio-frequency quadrupole mass spectrometer that measured both ion and neutral composition, in its OSI, and closed source neutral modes, respectively (Mandt et al., 2012; Teolis et al., 2010; Waite et al., 2004). The s/c velocity with respect to Saturn's corotation frame during the proximal orbits was close to 31 km/s, which corresponds to 25 times higher kinetic energy per nucleon for incident molecules than during the Titan encounters. Most of this speed can be attributed to the s/c motion in the inertial frame although there is some contribution from Saturn's rotation. INMS ion measurements at these speeds limit observable ion species to those with mass numbers less than 9 daltons (i.e., only lighter ions), whereas at Titan m/q up to 99 was measured. Details of the measurement of the light ion species can be found in Cravens et al. (2018).

For the OSI mode of INMS, ambient ions enter a small aperture from the ram direction within ≈3° across field of view (see Waite et al., 2004), and ion trajectories in the instrument are controlled by electrostatic potentials. Ions are deflected through a right angle by a quadrupole electrostatic lens (with voltages denoted QP3=-QP4) and are then directed into the mass analyzer. The QP3 voltage is normally adjusted for the expected ram speed for a range of different ion mass to charge ratios (m/q). For a mass number of 1 (protons) during P287, a special instrument mode was implemented during which the QP3 voltage was scanned through a range of values. This permitted the ion flux to be measured as a function of H^+ kinetic energy (giving the H^+ speed relative to the instrument or s/c).

The QP3 voltage is linearly related to the kinetic energy of incident ions (cf. Mandt et al., 2012; Waite et al., 2004). The coefficients in the linear relation were determined using laboratory calibrations and using energy scans carried out during a handful of Titan passes. Some uncertainty exists in the linear fit coefficients, but this did not significantly affect density determinations. In this paper we use two reasonable versions of the linear fits consistent with the various calibration activities. The "real" fit probably lies somewhere between the two cases listed below.

$$\text{Case (a) KE} = -(\text{QP3} + 53.49)/0.9281$$

$$\text{Case (b) KE} = -(\text{QP3} + 54.0)/0.9281.$$

KE is the kinetic energy of the ion in eV units, and QP3 is the lens voltage in volts, and the equations apply to any mass number, although in the current paper only m=1 (H^+) is relevant. The main effect of changing this relation is to systematically shift all derived speeds up or down by about 1 km/s (this will be discussed again later in the paper). The relative speeds between measurement points are only slightly affected.

2.2. Radio and Plasma Wave Science Electron Density Measurements

During P287, the Radio and Plasma Wave Science (RPWS) observed broadband electromagnetic whistler mode emissions. In low-density regions, these emissions are driven into resonance (the upper frequency cutoff) at the electron plasma frequency (f_p), from which the electron densities are derived (see Persoon et al., 2018). These densities are reported on later in the paper.

The RPWS Langmuir Probe (RPWS/LP) on Cassini also measured electron densities during P287 using current-voltage sweeps (reported on later in the Results section). The probe is a 5-cm radius sphere located on a 1.5-m boom. Fits to the measured sweeps are able to provide electron densities and temperatures, s/c potentials, and other quantities (see Gurnett et al., 2005; Hadid et al., 2018; Wahlund et al., 2018). RPWS/LP also measured electron densities using a continuous 20-Hz mode.

3. Proximal Orbit Geometry

For the proximal orbits the s/c entered the atmosphere in the northern hemisphere, crossed the ring plane (equatorial plane), reached closest approach (CA) in the southern hemisphere at latitude λ ≈ -7°, and then

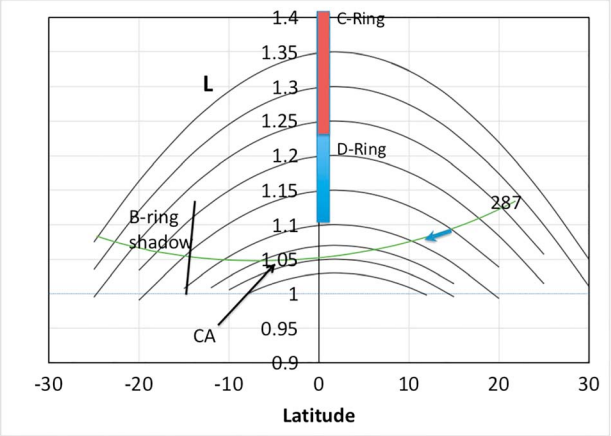

Figure 1. Geometry schematic. Shifted dipole magnetic field lines versus radial distance (L) and latitude, and Cassini trajectories for proximal orbit 287 are shown. Approximate locations of the C and D rings are shown, as is a possible proton velocity vector near 10°N latitude (see text). The approximate location of the B-ring shadow is indicated.

exited the atmosphere in the southern hemisphere. The s/c mainly moved from the north to the south when it was near Saturn. The maximum neutral density was also found at a latitude of $\lambda \approx$ -7°. For comparison, CA for P288 was an altitude of $z \approx$ 1,700 km, and for P287 CA was located at $z \approx$ 2,800 km. The radial distance of the s/c versus latitude is shown in Figure 1 for P287. Magnetic field lines from a simple displaced dipole field model are also shown (cf, Dougherty et al., 2018). Other features of the figure will be discussed later.

4. Results: Densities and Spacecraft Potential

4.1. Electron and Ion Densities

Figure 2 shows ion densities measured by INMS and RPWS and electron densities measured by RPWS as functions of latitude. Altitudes can be found from Figure 1. Not surprisingly, the maximum densities ($n_e = n_i \approx 400$ cm^{-3}) were reached near CA near -7° latitude. For P288 the maximum electron density measured ($\approx 10^4$ cm^{-3}) was about a factor of 10 higher than for P287 due to the lower altitudes (cf. Cravens et al., 2018). The largest densities are at the lowest altitudes, also corresponding to lower latitudes. The figure shows that the major ion species is H^+, except right near CA where H_3^+ is also present.

4.2. Spacecraft Potential

The RPWS/LP also used the voltage sweeps to determine the s/c potential Φ_{sc}, shown in Figure 3. Φ_{sc} was used to adjust deduced H^+ speeds measured by the INMS. For example, negative potentials will accelerate protons toward the s/c (and the INMS) and the resulting extra speed needs to be removed to correctly determine the ambient proton speed. s/c potential is determined by the balance of electrical currents entering or leaving the s/c, mainly by photoemission of electrons, and fluxes of ambient electrons and ions (Cully et al., 2007). Typically in an ionosphere, the equilibrium s/c potential is roughly the ambient electron thermal energy ($k_B T_e$, where k_B is Boltzmann's constant and T_e is the electron temperature).

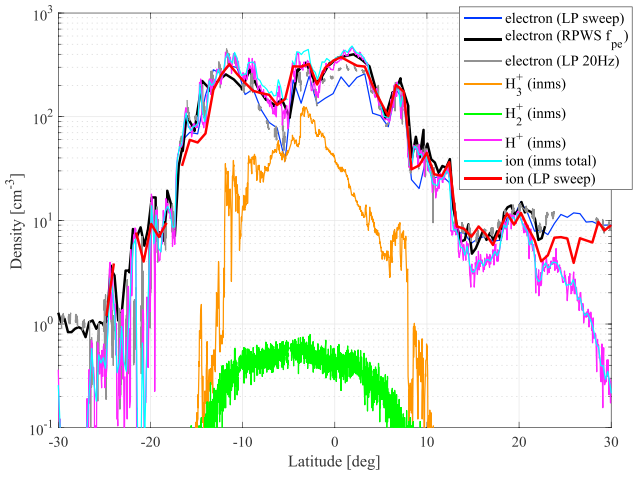

Figure 2. Total light ion density measured by the Cassini Ion and Neutral Mass Spectrometer and electron density from the Radio and Plasma Wave Science versus latitude. Also shown are H_2^+, H_3^+, and H^+ densities measured by Ion and Neutral Mass Spectrometer. Closest approach is at an altitude of 2,800 km and is at latitude -7°. The curve labeled Radio and Plasma Wave Science f_p shows densities measured using the plasma frequency.

5. Results: Ion Speeds

5.1. INMS Energy Scans

Figure 4 displays results from the P287 energy scans for the first QP/KE relation mentioned earlier. The case (a) QP/KE relation is used for this figure. The energy is converted to H^+ speed (relative to the instrument). The instrumental count rate per integration period for m=1 versus proton speed is shown for several latitudes. The scan curves all have a half-width of $\delta v \approx$ 3 km/s, which is a combination of instrumental velocity spread plus the thermal speed of the ionospheric protons. The peak count rate correlates with proton density (see Waite et al., 2004). For negative (south) latitudes the scan curves have their maxima near $v \approx$ 31.5 km/s. However, for northern latitudes, the measured speeds are closer to $v \approx$ 28 km/s.

The relative statistical accuracy of the points in Figure 4 is roughly the inverse of the square root of the counts. The statistical uncertainty is better than 1% for most of the scans and no worse than a few percent for the lowest count rates.

The speeds corresponding to the maximum count rate for each curve can be determined with some uncertainty. Figures 5a and 5b show a good and a not-so-good Gaussian fit, respectively, to one of the measured sets of energy scan points. Again, this is for case (a) QP/KE. Both Gaussian curves have a standard deviation of 3.2 km/s. The center speed of the two Gaussian curves is different by 0.9 km/s. Clearly, in this case the

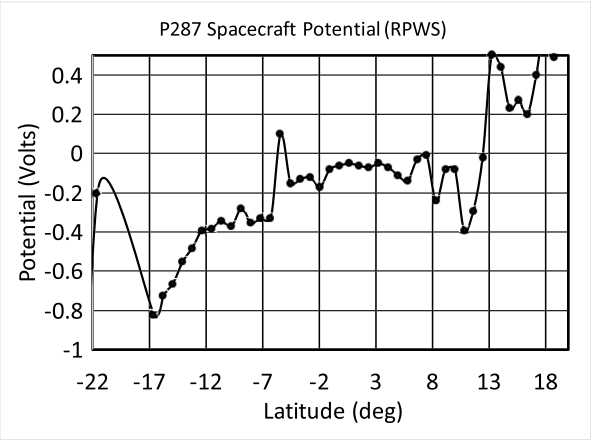

Figure 3. Spacecraft electrical potential measured by the Cassini Radio and Plasma Wave Science (RPWS)/Langmuir probe versus latitude. The potential values are between about -0.4 and + 0.4 V, for latitudes between about – 12 and +12°.

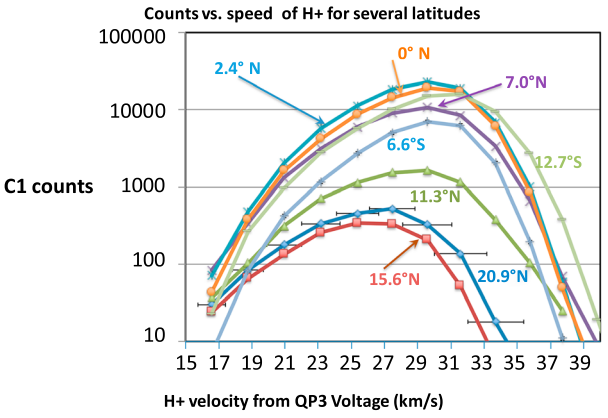

Figure 4. Ion and Neutral Mass Spectrometer energy scans for P287. Ion and Neutral Mass Spectrometer instrumental counts for H^+ ions per integration period plotted versus H^+ speed for several times/locations along the spacecraft track. Labeled with latitude. The statistical error is about 10% for counts of about 100 and is about 1% for the curves with the highest counts. Example statistical error bars are located on the left side of the figure.

maximum speed v_{max}=30.9 km/s works best. We estimate a conservative uncertainty of finding v_{max} of ≈ 0.5 km/s. Note that Gaussians do not have exactly the right shape to fit the data, particularly in the wings, but they help in finding the maximum speed.

Figure 6a shows v_{max} versus latitude for case (a). The speed is ≈ 31 km/s for latitudes less than ≈ 10°N. The speed then decreases to ≈26.5 km/s for latitudes more northerly than 10°N. Figure 6b shows the results when the second QP/KE relation is used; comparison of Figures 6a and 6b indicates that all the derived speeds are shifted lower by 1.5 km/s. The speed of the Cassini Orbiter relative to Saturn's atmospheric frame is shown. In the next section we correct the derived speeds for s/c potential and also transform to Saturn's corotating atmospheric frame.

5.2. Proton Speeds in Saturn's Rotating Frame of Reference

The proton speeds derived in the previous section need to be corrected for s/c potential in order to get the correct ram speed of the ambient ions. For example, a negative potential will give an ion an extra acceleration toward the s/c (and INMS) resulting in a deduced kinetic energy (or speed) that is too large. The actual kinetic energy of incident ions is KE (actual) = KE (scan) + e Φ_{sc}, where Φ_{sc} is the s/c potential. The speed is the square root of 2KE (actual)/m, where m is the proton mass.

The proton speed in Saturn's reference rotating frame is needed so we subtracted the s/c velocity relative to this frame from the measured ram velocities (shown in Figure 6 but corrected for Φ_{sc}). Cassini was moving at about 30.5 km/s relative to the atmosphere near CA and somewhat less than this on entry and exit from the topside ionosphere. Figures 7a and 7b show the measured speeds in Saturn's reference frame versus latitude, both with and without corrections for Φ_{sc} and for the two QP/KE cases. Recall that the Cassini orbiter moved mainly in the north-south direction, and not zonally, so that the measured proton velocity is almost entirely in the N-S direction (i.e., meridional flow).

The potential values are relatively low between about −12 and +12° latitude (Figure 3), but outside this region the s/c potential makes a significant difference to the results. Without correction, the flow is northerly in the southern hemisphere with v ≈ 2 km/s and southerly in the northern hemisphere, also with v ≈ 1.5 km/s using the first QP/KE relation (Figure 7a). That is, the flow in both hemispheres would be toward the equator (or the ring plane). On the other hand, taking Φ_{sc} into account, the flow speed in the southern hemisphere is small (v ≈ 0) and southerly and v ≈ 2 km/s in the northern hemisphere beyond 10°N.

For the second QP/KE relation (Figure 7b), the potential corrected flow is about 1 km/s southward (and down) in the southern hemisphere and about 2.5 to 3 km/s southward (and upward) in the northern hemisphere for latitudes between 7 and 18° north. Figure 8 summarizes the experimental results for the two QP/KE cases.

Note that if one assumes that the plasma mainly flows along magnetic field lines, then at 10°N latitude a measured velocity of 2.5-3 km/s corresponds to a field-aligned speed of $v_{||}$≈ 2.5-3 km/s/cos α ≈ 4 km/s, where α ≈ 50° is the angle between the s/c velocity and the field line at 15° N. A flow component perpendicular to the s/c velocity vector (and also the INMS aperture) would not show up in the energy scan although it could reduce the count rate.

6. Discussion: Topside Ionospheric Flow

In this section we discuss why Saturn's ionospheric plasma might flow from the north to the south at high altitudes. First, the distribution of

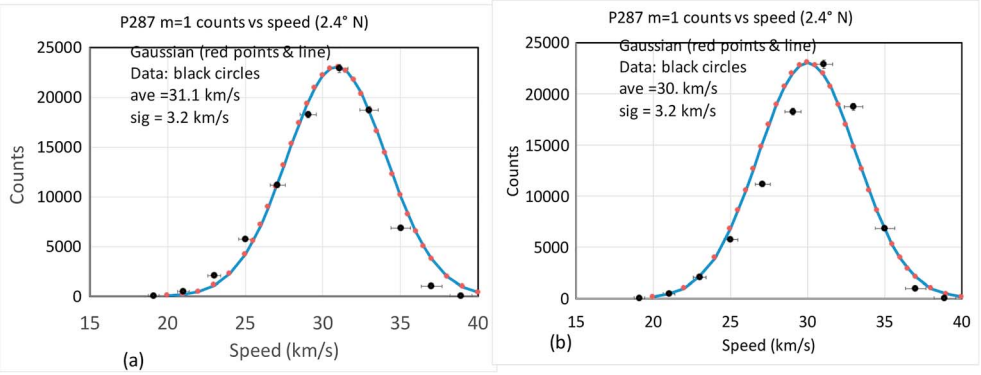

Figure 5. Gaussian fits for energy scan for a latitude of 2.5°N. Ion and Neutral Mass Spectrometer scan data are shown as points, and Gaussian curves shown as points and smooth lines. (a) Gaussian with center velocity of 31.1 km/s (b) Gaussian with center velocity of 30.0 km/s.

plasma should be affected by transport effects in regions where the chemical lifetime of an ion species is greater than the transport time (cf., Schunk & Nagy, 2009). As discussed by Cravens et al. (2018) and Moore et al. (2018), H^+ ions in Saturn's equatorial ionosphere are mainly chemically lost via reaction with heavy molecular neutrals (e.g., CH_4, H_2O, hydrocarbons ...) coming from the rings (cf. Perry et al., 2018; Waite et al., 2018). Adopting a rate coefficient of $k_c \approx 10^{-9}$ cm^3/s and a heavy species mixing ratio of $f \approx 10^{-4} - 10^{-3}$ the chemical lifetime is $\tau_c \approx 1/(k_c f n_{H2})$, where n_{H2} is the atmospheric H_2 density, which depends on altitude and latitude. The transport time is given by $\tau_T \approx L/v$, where L is the relevant length-scale (e.g., scale height or distance along the magnetic field). The flow speed depends on the forces on the plasma including pressure forces, gravity, and ion-neutral collisions.

Plasma flows in response to the net force on a fluid parcel. We assume that the ionospheric flow is along magnetic field lines and s is distance along a field line. The flow speed (along the field) is denoted u. The following single fluid momentum equation approximates this force balance (cf., Cravens et al., 2017):

$$\frac{d}{ds}\left[\rho u^2 + p\right] = -\rho\nu u - \rho g_{\parallel} \tag{1}$$

The mass density is denoted ρ and is given by $\rho = n_e\, m_p$ in the topside ionosphere, where n_e is the electron (and proton) density and m_p is the proton mass. The thermal pressure is denoted p and includes both electron and ion contributions: $p_e = n_e k_B T_e$ and $p_i = n_e\, k_B T_i$, where k_B is the Boltzmann constant and T_e and T_i are

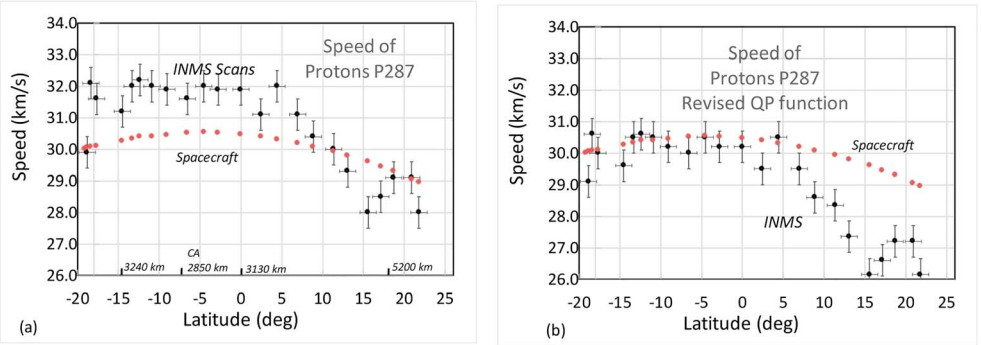

Figure 6. a) The bulk speed of H^+ ions relative to the Ion and Neutral Mass Spectrometer (INMS) aperture versus latitude as measured by INMS using the energy scans. The Cassini Orbiter speed relative to Saturn's atmosphere is also shown in both panels. Speeds determined using case (a) of the QP/KE relation. An altitude scale is shown at the bottom. CA denotes closest approach. b) Speeds determined using the case (b) QP/KE relation. The estimated uncertainty between points is shown by the error bars on each point.

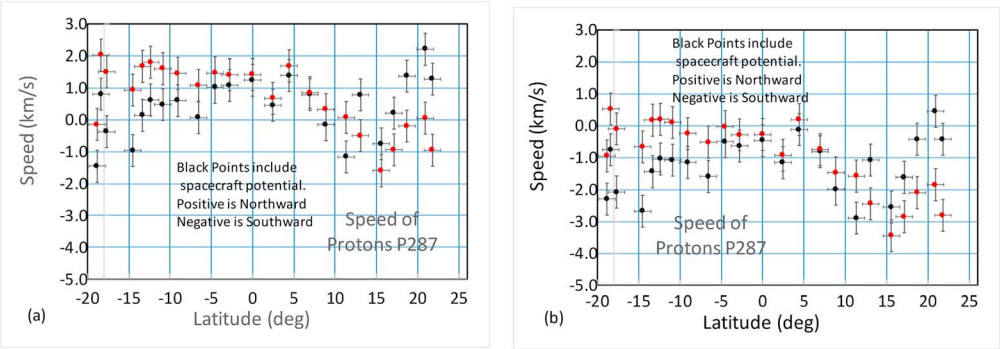

Figure 7. Bulk speed of protons relative to Saturn's rotating frame with (red points) and without (black points) spacecraft potential taken into account. (a) Determined using one version of QP/KE relation. (b) Determined using a slightly different QP/KE relation.

the electron and ion temperatures, respectively. Note that the plasma is assumed to be quasi-neutral so that $n_e = n_i$, where n_i is the ion density. The ion-neutral momentum transfer collision frequency is given by $\nu = k_{in}\, n_n$, where n_n is the neutral density and $k_{in} \approx 10^{-9}$ cm^3/s is a collision coefficient (Schunk & Nagy, 2009). The component of the gravitational acceleration along the magnetic field **B** is $g_{||}$. Cravens et al. (2018) applied the same equation to Mars but included the magnetic forces. The RPWS/LP measured the ionospheric electron temperature to be $T_e \approx 1{,}000$ K (Wahlund et al., 2018), and we assume that the ion temperature is approximately the neutral temperature, $T_i \approx T_n \approx 500$ K.

Numerical solutions to the fluid equations, including equation (1) plus continuity and energy equations, are needed for an accurate understanding of Saturn's topside ionosphere, but some simple statements will be made here. At low altitudes the collision term is large and the flow speed should be quite small. An ambipolar diffusion approximation would apply (cf. Cravens, 1997):

$$u \approx \frac{dp}{ds}\frac{1}{\rho\nu} \approx \frac{k_B\,(T_e + T_i\,)}{H_p\left(m_p k_{in} n_n\right)} \approx \frac{10\ m/s}{\left[\frac{n_n(cm^{-3})}{10^9 cm^{-3}}\right]} \tag{2}$$

The ambipolar diffusion approximation assumes that pressure forces, gravity forces, etc., are all balanced by ion-neutral fraction, and inertial terms in the momentum equation are neglected. The peak neutral density for P287 (Waite et al., 2018) is about 10^7 cm^{-3}, in which case equation (2) gives an estimated (and probably upper limit) theoretical flow speed of $u \approx 1$ km/s, kept low due to the effects of ion-neutral friction. Figure 7b is more in line with this expectation than is Figure 7a, Also, Figure 8b is more favored than Figure 8a.

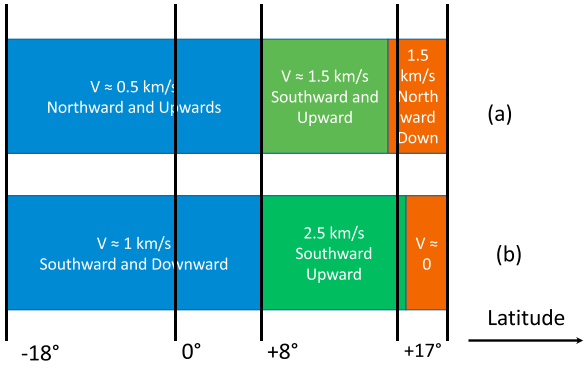

Figure 8. (a and b) Schematic outlining the velocity results (in Saturn's atmospheric frame) for the two Ion and Neutral Mass Spectrometer QP/KE scan cases discussed in the text. The authors believe that the case (b) is the more likely—low speeds for most latitudes but upward and southward in the northern hemisphere.

The plasma scale height was measured by RPWS with $H_p \approx 1500$ km (Persoon et al., 2018). Setting a transport time, $\tau_T \approx H_p/u$, equal to the H^+ chemical time, gives a transport to chemistry transition at an altitude where the neutral density is $n_n \approx 5 \times 10^7$ cm^{-3}. This time constant is about 5 hr, which is comparable to the 10-hr rotation period of Saturn. Diurnal effects are important in the topside ionosphere of Saturn.

At higher altitudes where ion-neutral friction is small, the following dynamical approximation should apply: $\rho u^2 + p \approx$ constant along a streamline (also a field line). An unbalanced pressure along B should lead to flow from high to low pressure according to this equation. In the extreme case of flow from a high-pressure region with $u \approx 0$ to a very low pressure region, the outflow speed can be estimated to be $u \approx C_s$, where the ion acoustic speed is given by $Cs = [k_B\,(T_e + T_i)/m_p]^{1/2}$. For Saturnian protons, $C_s \approx 5$ km/s, in line with the proton speed measured by the INMS near 10°N.

The flow scenario just discussed should apply if one end of the field line connecting conjugate hemispheres has low plasma density (and pressure) and the other end has higher density. But if the Saturnian atmosphere/ionosphere is sunlit at both ends, then an interhemispheric pressure gradient, and resulting flow, should not be present. For lower L-shell field lines whose latitudinal footprints in the lower ionosphere are less than 10-15° north or south, the ionosphere should be almost equally illuminated for both hemispheres and no net flow between them should exist (i.e., $u \approx 0$). On the other hand, as discussed by Hadid et al. (2018), the atmosphere for latitudes less than -15° is shadowed by the opaque B-ring. This might explain why Figure 7 shows plasma flow only for latitudes beyond ≈10°N. However, detailed modeling will be needed to settle this issue. Note that the C-ring shadow begins at about 7° south latitude, but the C-ring optical depth is only about 0.2.

Another issue is the diurnal variation of the topside ionosphere. A quick estimate shows that transport times along field lines near the equator are about the same as the length of day at Saturn, which affects the distribution of plasma along a field line, and thus flow speeds.

Another issue is the widths of the INMS-measured scan curves and shown in Figure 3. A Gaussian fit to the curves indicated a standard deviation of $\sigma = 3.1$ km/s at lower latitudes. σ is a combination of the instrumental width, σ_{inms}, and the thermal spread, σ_{th}: $\sigma^2 = \sigma_{inms}{}^2 + \sigma_{th}{}^2$. The instrumental width is roughly $\sigma_{inms} \approx 1.5 - 2$ km/s but was only poorly constrained by calibrations (Waite et al., 2004). Nominally, this would suggest that $\sigma_{th} \approx 2.5$ km/s very roughly. This value of σ_{th} corresponds to a H^+ temperature of $T_i \approx 500$ K, which is close to the neutral temperature of $T_n \approx 400$ K (Waite et al., 2018) as expected.

7. Summary

The most probable scenario (see Figure 8b) is that flow speeds are low (less than 1 km/s or so) for most latitudes but southward (and upward) at ≈ 3 km/s for northern latitudes beyond about 10°N. That is, the INMS energy scans for ionospheric protons made by the Cassini INMS during the P287 proximal orbit demonstrated that plasma is flowing from the topside ionosphere in the northern hemisphere to the topside ionosphere in the southern hemisphere for regions where the southern hemisphere is shadowed by the B-ring. Flow speeds of about 4 km/s along magnetic field lines were measured and are perhaps consistent with a simple plasma force balance analysis. The next step should be the construction of a numerical dynamical model of the low-latitude ionosphere.

Acknowledgments
The research described in this paper has been supported by NASA prime contract NAS7-03001 under JPL subcontract 1405853 to the Southwest Research Institute and SWRI subcontract to the University of Kansas. The research at the University of Iowa was supported by NASA through contract 1415150 with the Jet Propulsion Laboratory. Please see the supporting information for data used in creating the figures.

References

Cravens, T. E. (1997). *Physics of Solar System Plasmas*. Cambridge, UK: Cambridge University Press. https://doi.org/10.1017/CB09780511529467

Cravens, T. E., Hamil, O., Houston, S., Bougher, S., Ma, Y., Brain, D., & Ledvina, S. (2017). Estimates of ionospheric transport and ion loss at Mars. *Journal of Geophysical Research: Space Physics*, *122*, 10,626–10,637. https://doi.org/10.1002/2017JA024582

Cravens, T. E., Moore, L., Waite, J. H., Jr., Perryman, R., Perry, M., Wahlund, J.-E., et al. (2018). The ion composition of Saturn's equatorial ionosphere as observed by Cassini. *Geophysical Research Letters*, *45*. https://doi.org/10.1029/2018GL077868

Cully, C. M., Ergun, R. E., & Eriksson, A. I. (2007). Electrostatic structure and spacecraft in tenuous plasma. *Journal of Geophysical Research*, *112*, A09211. https://doi.org/10.1029/200JA012269

Dougherty, M. K., Cao, H., Khurana, K. K., Hunt, G. J., Provan, G., Kellock, S., et al. (2018). Saturn's magnetic field revealed by the Cassini Grand Finale. *Science*, *362*(6410), 46. https://doi.org/10.1126/science.aat5434

Gurnett, D. A., Kurth, W. S., Hospodarsky, G. B., Persoon, A. M., Averkamp, T. F., Cecconi, B., et al. (2005). Radio and plasma wave observations at Saturn from Cassini's approach and first orbit. *Science*, *307*(5713), 1255–1259. https://doi.org/10.1126/science.1105356

Hadid, L. Z., Mooroka, W., Wahlund, J.-E., Persoon, A. M., Andrews, D., Shebanits, O., et al. (2018). Saturn's ionosphere: Electron density altitude profiles and D ring electrodynamic interaction from the Cassini Grand Finale. *Geophysical Research Letters*, *45*. https://doi.org/10.1029/2018GL078004

Kliore, A. J., Patel, I. R., Lindal, G. F., Sweetnam, D. N., & Hotz, H. B. (1980). Structure of the ionosphere and atmosphere of Saturn from Pioneer 11 Saturn radio occultation. *Journal of Geophysical Research*, *85*(A11), 5857–5870. https://doi.org/10.1029/JA085iA11p05857

Koskinen, T. T., Sandel, B. R., Yelle, R. V., Strobel, D. F., Mueller-Wodarg, I. C. F., & Erwin, J. T. (2015). Saturn's variable thermosphere from Cassini/UVIS occultations. *Icarus*, *260*, 174–189. https://doi.org/10.1016/j.icarus.2015.07.008

Mandt, K., Gell, D., Perry, M., Waite, J. H., Crary, F., Young, D., et al. (2012). Ion densities and composition of Titan's upper atmosphere derived from the Cassini Ion Neutral Mass Spectrometer: Analysis methods and comparison of measured ion densities to photochemical model simulations. *Journal of Geophysical Research*, *117*, E10006. https://doi.org/10.1029/2012JE004139

Mitchell, D., Perry, M. E., Hamilton, D. C., Westlake, J. H., Kollmann, P., Smith, H. T., et al. (2018). D-ring dust falling into Saturn's equatorial upper atmosphere. *Science*, *362*(6410), 50. https://doi.org/10.1126/science.aat2236

Moore, L., Cravens, T. E., Mueller-Wodarg, I., Perry, M., Waite, J. H. Jr., Perryman, R., et al. (2018). Models of Saturn's equatorial ionosphere based on in situ data from Cassini's Grand Finale. *Geophysical Research Letters*, *45*, 9398–9407. https://doi.org/10.1029/2018GL078162

Perry, M. E., Waite, J. H. Jr., Mitchell, D. G., Miller, K. E., Cravens, T. E., Perryman, R. S., et al. (2018). Material flux from the rings of Saturn into its atmosphere. *Geophysical Research Letters*, *45*, 10,093–10,100. https://doi.org/10.1029/2018GL078575

Persoon, A. M., Kurth, W. S., Gurnett, D. A., Groene, J. B., Sulaiman, A. H., Wahlund, J.-E., et al. (2018). Electron density distribution in Saturn's ionosphere. *Geophysical Research Letters*, *46*, 3061–3068. https://doi.org/10.1029/2018GL078020

Schunk, R. W., & Nagy, A. F. (2009). *Ionospheres: Physics, Plasma Physics, and Chemistry* (2nd ed.). Cambridge, UK: Cambridge University Press. https://doi.org/10.1017/CBO9780511635342

Teolis, B., Perry, M., Magee, B., Westlake, J., & Waite, J. H. (2010). Detection and measurement of ice grains and gas distribution in the Enceladus plume by Cassini's Ion Neutral Mass Spectrometer. *Journal of Geophysical Research*, *115*, A09222. https://doi.org/10.1029/2009JA015192

Wahlund, J.-E., Morooka, M. W., Hadid, L. Z., Persoon, A. M., Farell, W. M., Gurnett, D. A., et al. (2018). In situ measurements of Saturn's ionosphere show that it is dynamic and interacts with the rings. *Science*, *359*(6371), 66–68. https://doi.org/10.1126/science.aao4134

Waite, J. H. Jr., Lewis, W. S., Kasprzak, W. T., Anicich, V. G., Block, B. P., Cravens, T. E., et al. (2004). The Cassini Ion and Neutral Mass Spectrometer (INMS) investigation. *Space Science Reviews*, *114*(1-4), 113–231. https://doi.org/10.1007/s11214-004-1408-2

Waite, J. H., Perryman, R. S., Perry, M. E., Miller, K. E., Bell, J., Cravens, T. E., et al. (2018). Chemical interactions between Saturn's atmosphere and its rings. *Science*, *362*(6410), 51. https://doi.org/10.1126/science.aat2382